Celorrio, V., Sebastian, D., Calvillo, L., Ana Beatriz, G., Fermin, D., & Lazaro, M. J. (2016). Influence of thermal treatments on the stability of Pd nanoparticles supported on graphitised ordered mesoporous carbons. International Journal of Hydrogen Energy, 41(43), 19570–19578. DOI: 10.1016/j.ijhydene.2016.05.271

Influence of thermal treatments on the stability of Pd nanoparticles supported on graphitised ordered mesoporous carbons

V. Celorrio[a, §], D. Sebastián[b, §], L. Calvillo[c], A.B. García[d], D.J. Fermin[a], M.J. Lázaro[e*]

[a] School of Chemistry. University of Bristol. Cantocks Close, Bristol BS8 1TS (UK)

[b] Istituto di Tecnologie Avanzate per l'Energia "Nicola Giordano", CNR, Via Salita S. Lucia sopra Contesse 5, 98126 Messina, Italy

[c] Dipartimento di Scienze Chimiche, Università di Padova, Via Marzolo 1, 35131 Padova, Italy.

[d] Instituto Nacional del Carbón, CSIC, Francisco Pintado Fe 26, 33011 Oviedo, Spain

[e] Instituto de Carboquímica, CSIC, Miguel Luesma Castán 4, 50018 Zaragoza, Spain

[§] These authors have contributed equally to the work.

* Corresponding author: Tel. +34 976 733977; Fax: +34 976 733318;

E-mail address: mlazaro@icb.csic.es

Keywords: ordered mesoporous carbon; graphitisation; corrosion; palladium; direct formic acid fuel cells

Abstract

The graphitisation of ordered mesoporous carbons (CMK-3) was carried out by thermal treatments under different conditions of temperature and heating rate. The electrochemical characterization in acidic medium of the graphitised CMK-3 showed that such a thermal treatment is effective to decrease the carbon oxidation rate (corrosion) while preserving a good porosity in terms of capacitance. Besides, the graphitisation degree and, in consequence, the electrochemical corrosion resistance can be modulated by an appropriate choice of thermal treatment conditions, where the heating rate and temperature appear as critical parameters. Under certain graphitisation conditions, the carbon corrosion of CMK-3 can be minimized showing lower rates compared to a commercial carbon black (Vulcan). Palladium nanoparticles were supported on the most promising graphitised CMK-3 and Vulcan using a method based on impregnation and reduction with borohydride, resulting in suitable metal crystallite sizes. The electrocatalytic activity towards the oxidation of carbon monoxide and formic acid were assessed in aqueous sulphuric acid electrolyte for application at the anode of direct formic acid fuel cells (DFAFCs). The best activity results were obtained for the Pd catalyst supported on a graphitised CMK-3.

1. Introduction

Among the different types of fuel cells, the most suitable for powering portable devices, electric vehicles and transportation, are the polymer electrolyte membrane and direct alcohol fuel cells, due to their low operating temperatures (60-100 °C) and fast start-up. In the case of alcohol fuel cells, in particular methanol, fuel crossover represents a major challenge which limits fuel concentration and overall energy density of the cell [1]. In this context, formic acid has emerged as an alternative fuel, showing lower crossover through the polymeric membrane than methanol [2], as well as for being non-carcinogenic, non-flammable and easy to store and transport.

The oxidation of formic acid (HCOOH) has been described to proceed through a dual pathway mechanism, which includes (i) its direct oxidation to CO_2, and (ii) an indirect pathway forming CO as an intermediate [3]. Although Pt is commonly used as fuel cell catalyst, previous studies showed that the rate of formic acid electrooxidation on pure Pt metal is insufficient for practical use, because Pt is severely poisoned by the adsorbed CO intermediate [4]. It has been demonstrated, however, that the use of Pt alloys can diminish this CO poisoning effect [5], especially alloys of Ru and Pd. It has also been established that Pd promotes the direct pathway for formic acid oxidation. Masel et al. demonstrated that unsupported Pd and Pd/C catalysts can overcome the CO poisoning effect, thereby yielding high performances in direct formic acid fuel cells (DFAFCs) [6, 7].

The electrooxidation of HCOOH on Pd nanostructures has been widely investigated in the literature [7-14]. Kolb et al. demonstrated that the electrocatalytic activity of Pd overlayers on Au and Pt single crystal electrodes depends markedly on their crystallographic orientation; following the trend Pd(111) < Pd(110) < Pd(100) [15, 16]. Although in previous studies the same authors showed that the activity of Pd nanostructures towards HCOOH oxidation is enhanced in the presence of a carbon support, leading to lower deactivation kinetics under potentiostatic conditions [13, 14, 17]; there is an intense discussion about the stability of Pd electrocatalysts under operational conditions of DFAFCs [18-21].

Carbon materials are the first choice for electrocatalyst supports because of their large specific surface area and high electrical conductivity. Carbon blacks, such as Vulcan XC-72 (220 m^2 g^{-1}), are widely considered as electrocatalyst support since they exhibit a good balance of physical properties. However, despite the need of a highly accessible surface area, other factors such as pore size distribution and surface chemistry also affect the properties and activity of noble metal electrocatalysts supported on carbon blacks. For these reasons, new carbon materials such as carbon nanofibers, ordered mesoporous carbons, carbon gels or carbon nanocoils, are being investigated in order to improve the electrochemical performance of the catalysts in the fuel cell [22, 23]. An important aspect regarding high surface area carbon supports is the irreversible corrosion occurring at highly positive potentials. In a fuel cell, the oxidation of carbon occurs mainly at the cathode side during operation at high electrode potentials like those arising in start-up/shut-down processes, and dominates the degradation of the membrane-electrode assembly [24, 25]. Moreover, the corrosion is accelerated under abnormal conditions like cell reversal, fuel starvation and sudden current transitions [26]. Recent investigations have also individuated an important corrosion phenomena at the anode side in transient operating conditions of fuel feeding [27]. The corrosion rate of carbon materials increases with their surface area, carbon disordering degree and with a high percentage of labile surface carbon moieties [28, 29]. However, the degradation rate can be significantly slowed down by graphitisation treatments at high temperature (1100-2000 °C) without compromising the advantage of a highly mesoporous texture [30-32].

Ordered mesoporous carbons (OMCs) have received great attention due to their unique properties, they can find potential applications in several fields [33-35]. They present a regular structure, high surface area, large pore volume and a narrow pore size distribution [33, 36]. Our group has previously studied CMK-3 carbons as electrocatalyst supports for fuel cells [37], however, a major disadvantage of these materials is the low electrical conductivity, which hinders the charge transfer.

In this work, we have studied how the graphitisation heat treatment affects mesoporous carbon materials to increase its resistance to corrosion and electrical conductivity. First, we synthesised two different types of ordered mesoporous carbons (CMK-3), followed by different thermal treatments. The electrochemical corrosion in acid medium of such graphitised OMCs was investigated. Pd nanoparticles were deposited on the most stable materials and the electrochemical activity towards CO and formic acid oxidations was studied.

2. Materials and methods

2.1. Synthesis of carbon materials, thermal treatment and characterization

Ordered mesoporous carbons (CMK-3-R2 and CMK-3-R8) were prepared by incipient wetness impregnation of SBA-15 silica with furan resin (Huttenes-Albertus) as carbon precursor. The silica materials SBA-15/R2 and SBA-15/R8 contained mass ratios of TEOS/P123 equal to 2 (R2) and 8 (R8). Subsequently, the impregnated silica was carbonized at 700 °C for 2 h, and the obtained silica-carbon composite was treated with HF (40 %, Fluka) to remove the silica, as described previously in [36, 38]. Finally, the carbon materials thus obtained were subjected to different thermal treatments. This treatment was carried out in a graphite electrical furnace for 1 h under argon flow.

Table 1 states the nomenclature and the heat treatment conditions used for the preparation of the carbon materials under study. Vulcan XC-72R (Cabot) and the untreated carbon materials were used to establish a comparison.

Table 1. Nomenclature and heat treatment conditions of the materials.

Material	Heating rate $^{o}C\ min^{-1}$	Temperature ^{o}C
CMK-3-R2	---	---
CMK-3-R2-1500-3	3	1500
CMK-3-R2-1500-5	5	1500
CMK-3-R2-1500-10	10	1500
CMK-3-R2-2000-5	5	2000
CMK-3-R8	---	---
CMK-3-R8-1500-10	10	1500
Vulcan	---	---

XRD patterns were recorded using a Bruker AXS D8 Advance diffractometer with a θ-θ configuration and using Cu Kα radiation. Raman spectra were obtained using a Horiba Jobin Yvon HR800 UV, using the green line of an argon laser (λ = 514.53 nm) as the excitation source.

The textural characteristics of the carbon materials supports were derived from the N_2 adsorption-desorption isotherms obtained at -196 ºC in a Micromeritics ASAP 2020 volumetric adsorption system. Specific surface area was calculated using the BET (Brunauer-Emmett-Teller) equation. Total pore volume was determined by the single point method at p/p_0=0.99. Micropore volume was assessed by applying the t-plot method.

The device designed to measure the electrical conductivity of carbon materials consisted of a polyethylene cylinder (electrical insulator), in which the sample was introduced. Two bronze pistons, connected to a current source (Time Electronics 1044) and a multimeter (Fluke 45 Dual display multimeter), were placed at both sides of the cylinder. An electrical current value of 19.99 mA was passed through the system, generating an electrical potential difference between both pistons. Meanwhile, a pressure in the interval 1-156 MPa was applied to the sample using a hydraulic press, to reach a maximum value of the electrical conductivity. The variation of the sample height inside the cylinder and the generated electrical potential difference were measured by a high precision laser device (Keyence LK-2101) and a multimeter, respectively. The value of the resistance was calculated by $R = \rho \cdot h/A$, where R is the electric resistance in Ω, ρ is the electric resistivity (Ω·cm), h the distance between the pistons (cm), and A the transversal section of the sample (cm^2). The electrical conductivity was calculated as $\sigma = h/A \cdot R$.

2.2. Corrosion experiments

Gas diffusion electrodes were prepared according to a procedure described elsewhere [39], consisting of carbon cloth backing, gas diffusion layer and the carbon layer under study. To reduce the flooding effects due to the use of a sulphuric acid aqueous solution electrolyte, a hydrophobic gas

diffusion layer was used (LT 1200W ELAT, E-TEK). The carbon layer was composed of 67 wt.% carbon (under study) and 33 wt.% Nafion® ionomer. The carbon loading was of *ca.* 0.65 mg cm^{-2} (±0.1 mg cm^{-2}) for all the electrodes.

Electrochemical corrosion tests were carried out in a conventional thermostated three-electrode cell consisting of the gas diffusion electrode to be tested (working electrode), a mercury-mercury(I) sulphate reference electrode (Hg/Hg_2SO_4, sat. K_2SO_4) and a high surface coiled platinum wire as counter electrode. The working electrode geometric area was 0.2 cm^2, and a 0.5 M H_2SO_4 aqueous solution was employed as electrolyte. Nitrogen was continuously fed to the electrode backing layer and to the electrolyte solution during the tests. An Autolab Metrohm potentiostat/galvanostat was used to perform the measurements.

An accelerated stress test was carried out for the evaluation of the carbon materials resistance to degradation [40]. It consisted of a potential holding at 1.2 V vs. RHE for 90 min, under inert atmosphere. The potential is high enough to cause carbon oxidation at reasonable currents but low enough to avoid the oxygen evolution reaction [28, 41]. Cyclic voltammograms at different scan rates (from 0.005 V s^{-1} to 0.1 V s^{-1}) and between 0.05 V and 0.8 V (vs. RHE) were recorded before and after the stress tests to estimate the capacitance of carbon materials. The capacitance has been calculated from the integration of the area enclosed by the voltammogram, dividing by two, thus obtaining the average value between charge and discharge processes. The average value obtained considering the different scan rates is then divided by the weight of porous carbon in the electrode. Blank experiments with the gas diffusion layer were performed to subtract its contribution to the capacitance.

2.3. Electrocatalysts synthesis and characterization

To prepare the electrocatalysts, Pd nanoparticles were firstly supported on the carbon materials following by reduction with $NaBH_4$, as described previously [42]. $Na_2PdCl_6 \cdot 4H_2O$ (98%, Sigma-Aldrich) was used as metal precursor to obtain a theoretical palladium loading of 20 wt.% on the different carbon materials.

The real content of Pd in the electrocatalysts was determined by energy dispersive X-ray (EDX) technique with a Röntec XFlash Si(Li) analyser, coupled to a scanning electron microscope Hitachi S-3400 N. X-ray diffraction (XRD) patterns were recorded in a Bruker AXS D8 Advance diffractometer with a θ-θ configuration and using Cu Kα radiation (λ = 0.154 nm). XRD scans were done for 2θ values between 20º and 100º. Nitrogen adsorption-desorption isotherms were obtained at 77 K using a Micromeritics ASAP 2020. The total surface area was determined by applying the Brunauer-Emmett-Teller (BET) equation, and the total pore volume was determined using the single-point method at p/p_0 = 0.99. Electrical conductivity measurements were performed as previously described in [43].

For the electrochemical characterization of the Pd catalysts, a two-compartment electrochemical cell was used with a Pt wire and a saturated Ag/AgCl as counter and reference electrodes, respectively. The reference electrode compartment was separated by a glass frit to avoid contamination from the reference electrode solution. To prepare the working electrodes, first, an ink of the electrocatalyst was made from 2 mg of the catalyst and 15 µL of Nafion dispersion (5 wt.%, Aldrich) in 500 µL of ultrapure water. Then, an aliquot of 40 µL of this mixture was deposited onto a glassy carbon disk electrode (7 mm diameter) and dried. Cyclic voltammograms were recorded with an Autolab PGSTAT30. All electrochemical experiments were performed multiple times and reproducible results were obtained.

Adsorbed CO oxidation voltammograms were measured employing highly pure CO (99.97%, CK Gas) in 0.5 M H_2SO_4 solutions. The charge associated with CO stripping from the saturated catalysts was used to measure the electrochemical active areas, employing a charge of 315 µC cm^{-2} per unit area [44]. Formic acid oxidation was characterized by cyclic voltammetry and chronoamperometry, recorded in 2 M HCOOH + 0.5 M H_2SO_4 solutions. Potentiostatic current density-time (*j*-*t*) curves were recorded at 0.60 V vs. RHE for 900 s. This potential is close to the characteristic operational potential in DAFC cells.

3. Results and discussion

3.1. Corrosion studies

The electrochemical corrosion of the different carbon materials has been investigated by chronoamperometry at 1.2 V vs. RHE in sulfuric acid at room temperature. The current-time curves, represented in Figure 1, have been fitted to the following equation according to the literature [45]:

$$j = k\, t^{-n} \qquad \text{(Eq. 1)}$$

where *j* is the anode current per unit mass of carbon, *t* represents time and *k* and *n* are constants. Carbon electrochemical corrosion at elevated potentials proceeds through the following reaction [41]:

$$C + 2\, H_2O \rightarrow CO_2 + 4\, H^+ + 4\, e^- \qquad (\varphi_{00} = 0.207 \text{ V vs. RHE}) \quad \text{(Eq. 2)}$$

The fitting parameters are summarized in Table 2. For the sake of comparison, a commercial carbon black (Vulcan) has been included in this study. Vulcan is recognized as the benchmark carbon support for fuel cell electrocatalysts.

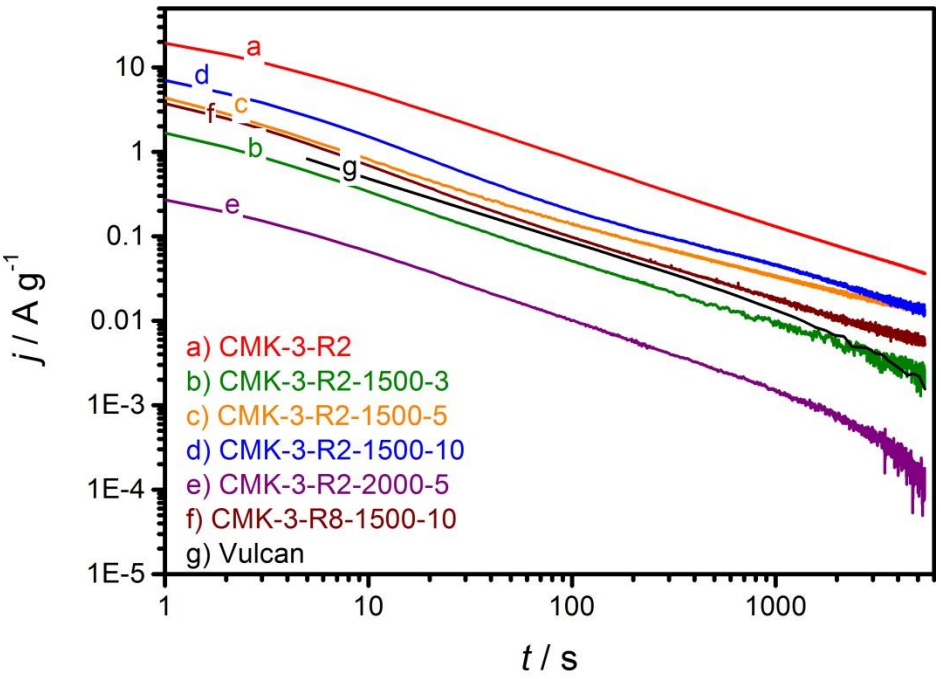

Figure 1. Current-time curves for the corrosion tests at 1.2 V vs. RHE, 0.5 M H_2SO_4, 0.65 mg cm^{-2} carbon loading, at room temperature.

Table 2. Corrosion parameters of the carbon materials.

Material	k	n	Carbon oxidation charge in 90 min	Capacitance (t = 0)	$\frac{C_{t=90} - C_{t=0}}{C_{t=0}}$
	A s^n g^{-1}		C g^{-1}	F g^{-1}	-
CMK-3-R2	33.3	0.80	768	61.0	0.477
CMK-3-R2-1500-3	2.1	0.81	53	6.1	0.199
CMK-3-R2-1500-5	4.7	0.77	178	20.7	0.402
CMK-3-R2-1500-10	11.5	0.89	244	26.9	0.480
CMK-3-R2-2000-5	0.43	0.82	8.5	0.76	0.199
CMK-3-R8-1500-10	4.7	0.84	107	14.0	0.437
Vulcan	2.9	0.78	106	4.3	0.463

All the carbon materials show a very similar corrosion mechanism, with *n* constant values around 0.8 (only for CMK-3-R2-1500-10 this value is significantly higher). The differences are encountered in the *k* constant values and, consequently, the charge, as well as the specific capacitance. The values of the constant *k* are a good indication of corrosion rate even if they are not dimensionally homogeneous (the units depend on the precise value of *n*). Nevertheless, similar slopes were found in Figure 1 (similar values of *n*) and, as a consequence, the k values reported can be considered a good index to analyse differences in corrosion resistance. On the other hand, the capacitance was estimated through cyclic voltammetry in the base electrolyte at increasing scan rates from 0.005 V s^{-1} to 0.1 V s^{-1}. The current corresponding to the hydrophobic gas diffusion layer (without carbon layer) was negligible, accounting three orders of magnitude lower than the thinnest carbon electrode based on Vulcan.

Regarding the various graphitisation conditions for the CMK-3s, it is remarkable that all of them significantly reduce their corrosion rate with respect to the pristine CMK-3-R2. The effect of heating rate is evident within the CMK-3s named CMK-3-R2 followed by 1500-3, 1500-5 and 1500-10, where a slow heating treatment clearly favours a higher corrosion resistance. A slower heating rate means a longer treatment during the heating ramp until achieving the steady-state temperature (1500 ºC). The graphitisation degree is known to be favoured with long treatment durations at high temperatures. Besides, the surface area of porous carbon materials might also diminish with graphitisation treatments, as envisaged from the variation of the specific capacitance, from 26.9 C g^{-}

^{1} for the CMK-3 treated with 10 ºC min^{-1} ramp to 6.1 C g^{-1} for the one treated at 3 ºC min^{-1}. It appears thus that the heating rate might influence both the graphitisation and the surface area leading to lower corrosion rates. The treatment temperature plays also an important role, as observed for CMK-3-R2-2000-5, showing the lowest rate constant, *k*, of 0.43 A s^{n} g^{-1}, in fact one order of magnitude lower than its counterpart CMK-3-R2-1500-5 (4.7 A s^{n} g^{-1}). Another important aspect regards the properties related to the mass ratio of TEOS/P123: the graphitised CMK-3-R8 presents a significantly lower corrosion rate than its counterpart CMK-3-R2. This is clearly correlated to the lower surface area of the CMK-3-R8 compared to the CMK-3-R2 (Table 3), which also leads to a lower electrochemical capacitance (Table 2).

When these materials are compared to the reference carbon material Vulcan (Table 2), two of the graphitised CMK-3s show a lower corrosion rate, namely those treated at 1500 °C with the lowest heating rate (CMK-3-R2-1500-3) and at 2000 °C (CMK-3-R2-2000-5). Taking into account their porous development, this represents a clear advantage towards their use in highly corrosive environments. In particular, Figure 2 represents the values obtained for the anodic charge within the first 90 min, correlated to the net amount of oxidized carbon, as a function of their electrochemical capacitance before the corrosion test. The capacitance is a good indicative of the practical electrochemical surface area of the electrodes, and hence, mainly depends on the carbon surface area among other less relevant parameters. One of the main parameters affecting carbon corrosion is the electrochemical surface area, among others (like the surface composition or the graphitisation degree). In practice, this means that the higher the exposed carbon surface, the higher the corrosion rate. In other words, a carbon material with high specific capacitance is more prone to corrosion unless its structure is more graphitic and/or there is a higher density of resistant surface carbon moieties [28, 29]. Apparently, the differences encountered in carbon corrosion among the graphitised CMK-3s of the present work are more correlated to the electrochemical surface area rather than other parameters like graphitisation or surface chemistry. In the subsequent section the relative influence of graphitisation level on corrosion rate will be briefly discussed on the basis of Raman spectra.

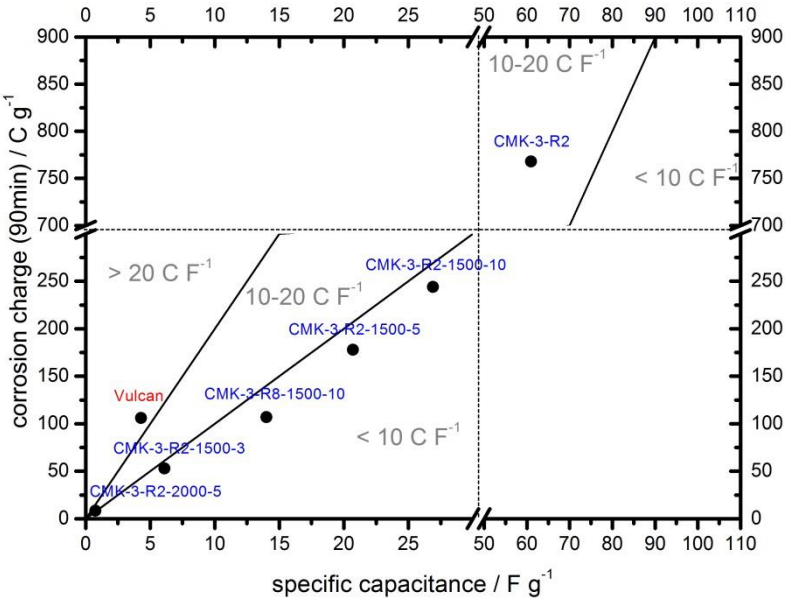

Figure 2. Corrosion charge dependence on capacitance for the different CMK-3s and Vulcan.

Three regions can be distinguished in Figure 2, as indicated by the straight lines: less than 10 C F^{-1}, between 10 and 20 C F^{-1} and higher than 20 C F^{-1}. Four of the graphitised CMK-3s are found within the zone of low specific corrosion charge: CMK-3-R2-1500-3, CMK-3-R8-1500-10, CMK-3-R2-1500-5 and CMK-3-R2-1500-10. The heating rate, and thus, the time of heating to reach the final temperature, appears as an important parameter towards CMK-3s corrosion behaviour and capacitance. As seen, both the corrosion charge and the capacitance decrease as this time increases, this is, in other words, the slower the heating slope, the more resistance to corrosion, but also the lower the capacitance of the carbon, maintaining the same charge to capacitance ratio.

Notice that the pristine mesoporous carbon, CMK-3-R2, which presents an intermediate the highest value of capacitance (61 C g^{-1}), is found in the region 10-20 C F^{-1}. Vulcan is, on the other hand, the carbon material with the highest corrosion charge (> 100 C g^{-1}) taking into account its low capacitance, (< 5 C g^{-1}). All the graphitised CMK-3s are found in the region < 10 C F^{-1}, as indicated in Figure 2, highlighting that the graphitisation treatment of CMK-3s represents a good opportunity

to tune corrosion characteristics without significant loss of the advantages coming from their peculiar porous structure.

3.2. Characterization of carbon materials and electrocatalysts

CMK-3-R8-1500-10 was chosen to be tested as an electrocatalysts' support for fuel cells, since it presented the best balance with a low corrosion rate and high electrochemical capacitance (7.6 C F^{-1}). For comparison, its counterpart CMK-3-R2-1500-10 and Vulcan were also used. The textural properties of the carbon supports are reported in Table 3. The first observation is the decrease of the specific surface area and the pore volume with the thermal treatment. Whereas CMK-3-R2 presents a high specific surface area of 893 m^2 g^{-1} and a pore volume of 0.60 cm^3 g^{-1}, CMK-3-R2-1500-10 has a specific surface area of 590 m^2 g^{-1} and a pore volume of 0.43 cm^3 g^{-1}. The same trend is observed for CMK-3-R8 and CMK-3-R8-1500-10. On the other hand, Vulcan XC-72R has a specific surface area of 218 m^2 g^{-1} and a pore volume of 0.41 cm^3 g^{-1}.

Table 3 also summarizes the electrical conductivity values for the different carbon supports. It can be observed that the thermal treatment increases the conductivity by an order of three, from ~ 0.01 S cm^{-1} for CMK-3-R2 and CMK-3-R8 to 11 and 23 S cm^{-1} for CMK-3-R2-1500-10 and CMK-3-R8-1500-10, respectively. Vulcan has a very high electrical conductivity (59 S cm^{-1}), which is one of the reasons because this material is used as commercial catalyst support for this application.

Table 3. Macroscopic and mesoscopic properties of the different carbon supports. The untreated CMK-3-R2 and CMK-3-R8 have been included for comparison.

Sample	A_{BET}	V_{total}	A_{Meso}	V_{Meso}	Electrical conductivity
	m^2 g^{-1}	cm^3 g^{-1}	m^2 g^{-1}	cm^3 g^{-1}	S cm^{-1}
CMK-3-R2	893	0.60	540	0.42	~ 0.01
CMK-3-R2-1500-10	590	0.43	42	0.10	11

CMK-3-R8	627	0.49	578	0.38	~ 0.01
CMK-3-R8-1500-10	282	0.27	25	0.06	23
Vulcan	218	0.41	153	0.38	59

Characteristic X-ray diffractograms obtained for the carbon materials and the Pd particles on the various carbon supports are illustrated in Figure 3. Figure 3a displays the XRD patterns of carbon materials and Vulcan. A peak around $2\theta = 24.85^{o}$ corresponding to the (002) reflection characteristic of graphite, can be observed, confirming that Vulcan has an intermediate structure between amorphous and graphitic, called turbostratic structure. CMK-3-R2-1500-10 and CMK-3-R8-1500-10 materials also show the (002) reflection in their XRD patterns, however, it appears broader and shifted to lower angles (24.6^{o}), indicative of their more amorphous character. Figure 3b shows the diffraction patterns obtained for the Pd catalysts prepared. Signals observed at 39.4^{o}, 45.6^{o}, 67.41^{o} and 81.31^{o} can be associated with the (111), (200), (220) and (311) Pd planes, respectively.

Figure 3c shows the Raman spectra for the selected carbon supports. The typical disordered (D) and graphitic (G) bands were obtained for the CMK-3s, characterized by different TEOS/P123 ratios but the same graphitisation treatment. The main difference is observed to be the relative intensities between them, named I_D/I_G, being slightly higher for the R2 carbon material (1.43). A lower intensity ratio for the R8 carbon (1.16) indicates a higher ordering degree. The latter CMK-3 presented a lower corrosion-related charge of 107 C g^{-1} (see Table 2) when compared to the R2 (244 C g^{-1}) but also a lower initial capacitance (14 vs. 26.9 F g^{-1}). Normalizing the corrosion charge by the specific capacitance, the R8 carbon shows a slightly lower specific corrosion rate (7.6 C F^{-1}) compared to the R2 (9.1 C F^{-1}), which points to the positive contribution of the CMK-3 graphitisation level on lowering the corrosion rate.

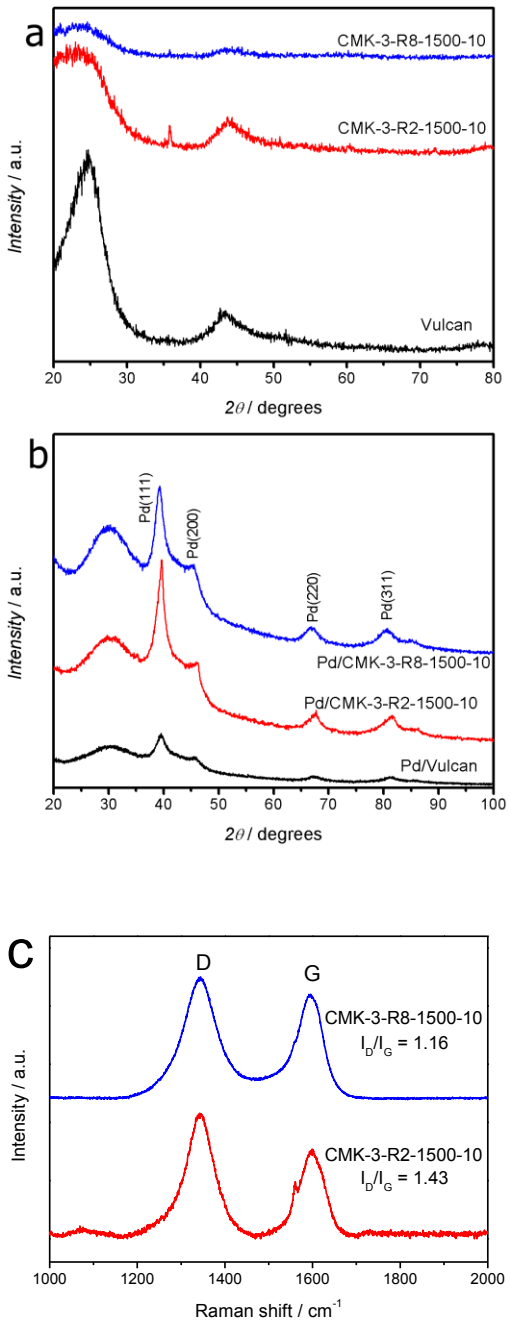

Figure 3. XRD patterns for the carbon materials used as supports (a) and for the Pd catalysts prepared (b). Raman spectra for the carbon materials used as supports (c).

The average Pd crystallite size (*d*) was calculated by the Scherrer equation using the (220) peak from XRD (Figure 3b) and the values are summarized in Table 4. As can be seen, similar particle size was obtained when the different graphitised CKM-3 were used as support. Assuming that Pd particles are spherical, the surface area (SA) can be calculated by the equation SA ($m^2\ g^{-1}$) = $6 \cdot 10^3/\rho d$,

where d is the mean metal crystallite size in nm, and ρ is the density of Pd (11.9 g cm^{-3}). The largest SA corresponds to Pd/CMK-3-R2-1500-10 and Pd/Vulcan due to their smaller crystallite size. For this reason, it would be expected that the highest activity towards formic acid oxidation would be achieved by these materials due to the more available surface area. However, the SA is not the only parameter influencing the activity of the catalysts, and as we should demonstrate later, this is not the case.

Table 4. Average crystallite sizes (d) of the Pd nanoparticles as estimated from XRD analysis, metal surface areas and electrochemical active areas (ECSA).

Catalyst	d nm	SA $m^2\ g^{-1}$	ECSA cm^2
Pd/CMK-3-R2-1500-10	5.0	101	8.0
Pd/CMK-3-R8-1500-10	6.0	84	6.0
Pd/Vulcan	5.0	101	9.8

The voltammetric features associated with CO stripping at Pd/CMK-3-R2-1500-10, Pd/CMK-3-R8-1500-10 and Pd/Vulcan electrocatalysts are contrasted in Figure 4. The hydrogen adsorption region appears blocked in the initial forward scan due to adsorbed CO at the Pd surface. The disappearance of the CO stripping peak on subsequent scans, and the reappearance of hydrogen peaks at more negative potentials, indicate complete removal of CO in the first scan. The key feature in Figure 4 is the CO stripping peak located at ~0.90 V in the Pd/Vulcan and Pd/CMK-3-R8-1500-10 catalysts. For Pd/CMK-3-R2-1500-10 this peak is shifted 50 mV to more positive potentials, indicating the lowest catalytic activity. Values of the electrochemical active areas are reported in Table 4.

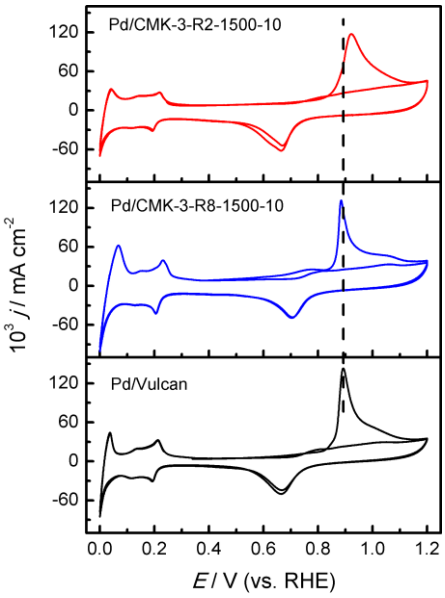

Figure 4. CVs for the oxidation of a monolayer of CO adsorbed at 0.2 V vs. RHE on the Pd electrocatalysts supported on the different carbon materials at a scan rate of 0.02 V s^{-1}. The currents have been normalized by the electrochemical active surface area determined from the CO-stripping.

Formic acid oxidation was studied using cyclic voltammetry and chronoamperometry. Cyclic voltammograms were recorded in 2 M HCOOH + 0.5 M H_2SO_4, at a scan rate of 0.02 V s^{-1}. Cyclic voltammograms showing the oxidation of formic acid at Pd/Vulcan and Pd/CMK-3-R2-1500-10 and Pd/CMK-3-R8-1500-10 are contrasted in Figure 5. All three catalysts presented a broad peak on the forward scan and a drop in current as Pd oxide is formed, inhibiting further formic acid oxidation. On the backward scan, once the Pd surface is recuperated, formic acid is once again oxidized. Similar current densities were obtained on the forward and backward scans, indicating a high tolerance towards electrode poisoning [46]. Somewhat lower currents were obtained on Pd/Vulcan and Pd/CMK-3-R2-1500-10 than on Pd/CMK-3-R8-1500-10 electrocatalysts.

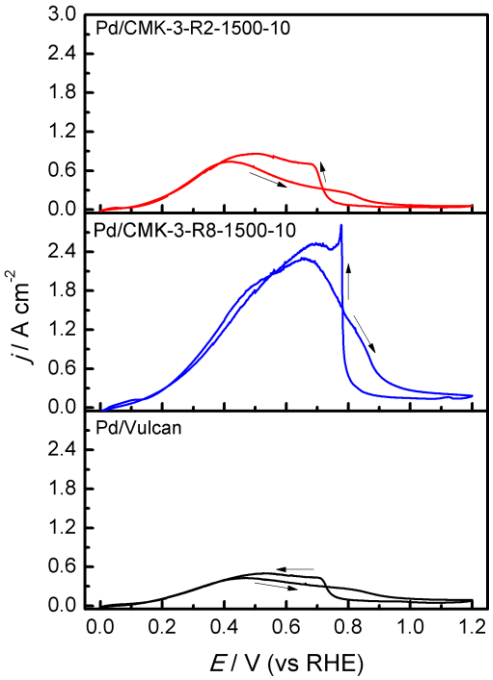

Figure 5. Cyclic voltammograms of the different Pd electrocatalysts in presence of 2 M HCOOH + 0.5 M H_2SO_4, at 0.02 V s^{-1}. The currents have been normalized by the electrochemical active surface area determined from the CO-stripping.

Potentiostatic current density - time (*j-t*) curves were recorded in the same solution, at 0.60 V, for 900 s. Chronoamperometric transients at 0.6 V are compared in Figure 6. All the chronoamperograms are characterized by a decrease of the current with time, associated with the deactivation of the electrocatalysts. The deactivation rate appears similar for Pd/Vulcan and Pd/CMK-3-R2-1500-10 catalysts. However, it seems rather slower for Pd/CMK-3-R8-1500-10. It should be noticed that the relative changes in the current densities from the chronoamperograms are consistent with the cyclic voltammograms (Figure 5). From this analysis, it emerged that the most active catalyst is Pd/CMK-3-R8-1500-10, probably due to its high electrical conductivity and highly ordered structure.

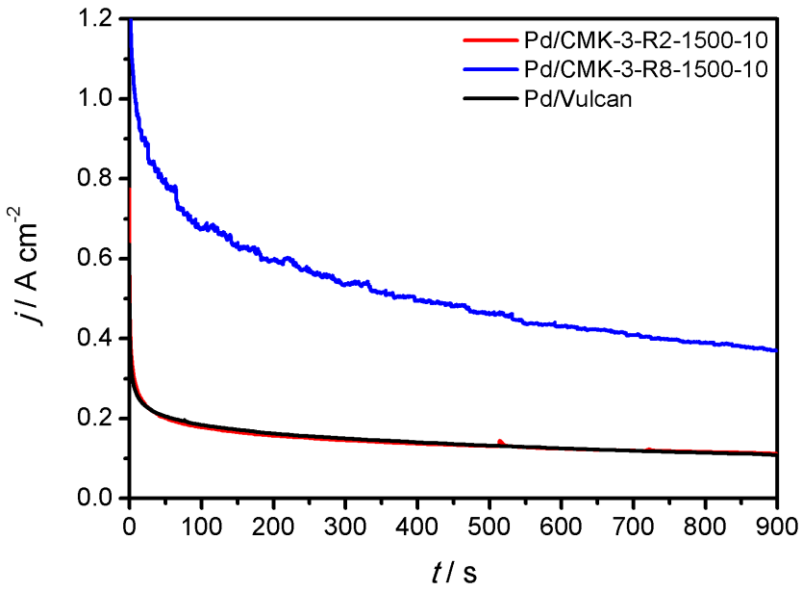

Figure 6. Current-time curves for formic acid oxidation in 2 M HCOOH + 0.5 M H_2SO_4 on the Pd electrocatalysts supported on different carbon materials at 0.6 V vs. RHE and room temperature. The currents showed have been normalized by the electrochemical active surface area determined from the CO-stripping.

4. Conclusions

Ordered mesoporous carbon materials (CMK-3s) have been prepared and thermally treated at temperatures in the interval 1500-2000 ºC. Such a graphitisation treatment has been shown to be effective to reduce the electrochemical corrosion rate. In comparison to a widely used carbon black (Vulcan), even lower carbon oxidation rates can be achieved by an appropriate selection of the graphitisation conditions. Moreover, the corrosion of carbon is strongly correlated to the thermal treatment conditions, allowing to attain mesoporous carbon materials which showed to be more resistant to corrosion phenomena.

Pd nanoparticles have been deposited on the most promising CMK-3s and on the commercial carbon black for comparison purposes. The catalysts showed an appropriate crystallite size of about 5 nm. Their electrocatalytic activity towards CO and HCOOH oxidation has been investigated by cyclic

voltammetry and chronoamperometry in acidic medium. The highest electrocatalytic activity was found for the Pd catalyst supported on the graphitized CMK.

Acknowledgements

The authors want to thank the Spanish Ministry of Economy and Competitiveness and FEDER for financial support under the project ENE2014-52158-C2-1-R. V. Celorrio also acknowledges the Royal Society and the UK National Academy by the support through the Newton International Fellows program.

References

[1] Liu Z, Hong L, Tham MP, Lim TH, Jiang H. Nanostructured Pt/C and Pd/C catalysts for direct formic acid fuel cells. J Power Sources. 2006;161:831-5.
[2] Chen M, Wang ZB, Zhou K, Chu YY. Synthesis of Pd/C Catalyst by Modified Polyol Process for Formic Acid Electrooxidation. Fuel Cells. 2010;10:1171-5.
[3] Capon A, Parsons R. The oxidation of formic acid at noble metal electrodes Part III. Intermediates and mechanism on platinum electrodes. J Electroanal Chem. 1973;45:205-31.
[4] Jiang J, Kucernak A. Nanostructured platinum as an electrocatalyst for the electrooxidation of formic acid. J Electroanal Chem. 2002;520:64-70.
[5] Capon A, Parsons R. The oxidation of formic acid at noble metal electrodes Part 4. Platinum + palladium alloys. J Electroanal Chem. 1975;65:285-305.
[6] Ha S, Larsen R, Masel RI. Performance characterization of Pd/C nanocatalyst for direct formic acid fuel cells. J Power Sources. 2005;144:28-34.
[7] Larsen R, Ha S, Zakzeski J, Masel RI. Unusually active palladium-based catalysts for the electrooxidation of formic acid. J Power Sources. 2006;157:78-84.
[8] Zhang L, Lu T, Bao J, Tang Y, Li C. Preparation method of an ultrafine carbon supported Pd catalyst as an anodic catalyst in a direct formic acid fuel cell. Electrochem Commun. 2006;8:1625-7.
[9] Huang Y, Zhou X, Liao J, Liu C, Lu T, Xing W. Preparation of Pd/C catalyst for formic acid oxidation using a novel colloid method. Electrochem Commun. 2008;10:621-4.
[10] Hu C, Bai Z, Yang L, Lv J, Wang K, Guo Y, et al. Preparation of high performance Pd catalysts supported on untreated multi-walled carbon nanotubes for formic acid oxidation. Electrochim Acta. 2010;55:6036-41.
[11] Wang R, Liao S, Ji S. High performance Pd-based catalysts for oxidation of formic acid. J Power Sources. 2008;180:205-8.
[12] Yunjie H, Jianhui L, Changpeng L, Tianhong L, Wei X. The size-controlled synthesis of Pd/C catalysts by different solvents for formic acid electrooxidation. Nanotechnology. 2009;20:105604.
[13] Celorrio V, Montes de Oca MG, Plana D, Moliner R, Lázaro MJ, Fermín DJ. Effect of Carbon Supports on Electrocatalytic Reactivity of Au–Pd Core–Shell Nanoparticles. J Phys Chem C. 2012;116:6275-82.
[14] Montes de Oca MG, Plana D, Celorrio V, Lazaro MJ, Fermín DJ. Electrocatalytic Properties of Strained Pd Nanoshells at Au Nanostructures: CO and HCOOH Oxidation. J Phys Chem C. 2012;116:692-9.
[15] Baldauf M, Kolb DM. Formic Acid Oxidation on Ultrathin Pd Films on Au(hkl) and Pt(hkl) Electrodes. J Phys Chem. 1996;100:11375-81.
[16] Hoshi N, Kida K, Nakamura M, Nakada M, Osada K. Structural Effects of Electrochemical Oxidation of Formic Acid on Single Crystal Electrodes of Palladium. J Phys Chem B. 2006;110:12480-4.

[17] Celorrio V, Montes de Oca MG, Plana D, Moliner R, Fermín DJ, Lázaro MJ. Electrochemical performance of Pd and Au–Pd core–shell nanoparticles on surface tailored carbon black as catalyst support. Int J Hydrogen Energy. 2012;37:7152-60.
[18] Yu X, Pickup PG. Mechanistic study of the deactivation of carbon supported Pd during formic acid oxidation. Electrochem Commun. 2009;11:2012-4.
[19] Yu X, Pickup PG. Deactivation/reactivation of a Pd/C catalyst in a direct formic acid fuel cell (DFAFC): Use of array membrane electrode assemblies. J Power Sources. 2009;187:493-9.
[20] Jung WS, Han J, Yoon SP, Nam SW, Lim T-H, Hong S-A. Performance degradation of direct formic acid fuel cell incorporating a Pd anode catalyst. J Power Sources. 2011;196:4573-8.
[21] Zhou Y, Liu J, Ye J, Zou Z, Ye J, Gu J, et al. Poisoning and regeneration of Pd catalyst in direct formic acid fuel cell. Electrochim Acta. 2010;55:5024-7.
[22] Gálvez ME, Calvillo L, Alegre C, Sebastián D, Suelves I, Pérez-Rodríguez S, et al. Nanostructured Carbon Materials as Supports in the Preparation of Direct Methanol Fuel Cell Electrocatalysts. Catalysts. 2013;3:671-82.
[23] Lázaro MJ, Ascaso S, Pérez-Rodríguez S, Calderón JC, Gálvez ME, Jesús Nieto M, et al. Carbon-based catalysts: Synthesis and applications. CR Chimie. 2015;18:1229-41.
[24] Castanheira L, Dubau L, Mermoux M, Berthomé G, Caqué N, Rossinot E, et al. Carbon Corrosion in Proton-Exchange Membrane Fuel Cells: From Model Experiments to Real-Life Operation in Membrane Electrode Assemblies. ACS Catalysis. 2014;4:2258-67.
[25] Borup R, Meyers J, Pivovar B, Kim YS, Mukundan R, Garland N, et al. Scientific Aspects of Polymer Electrolyte Fuel Cell Durability and Degradation. Chem Rev. 2007;107:3904-51.
[26] Zhang S, Yuan X, Wang H, Mérida W, Zhu H, Shen J, et al. A review of accelerated stress tests of MEA durability in PEM fuel cells. Int J Hydrogen Energy. 2009;34:388-404.
[27] Engl T, Gubler L, Schmidt TJ. Fuel Electrode Carbon Corrosion in High Temperature Polymer Electrolyte Fuel Cells—Crucial or Irrelevant? Energy Technology. 2015:n/a-n/a.
[28] Artyushkova K, Pylypenko S, Dowlapalli M, Atanassov P. Structure-to-property relationships in fuel cell catalyst supports: Correlation of surface chemistry and morphology with oxidation resistance of carbon blacks. J Power Sources. 2012;214:303-13.
[29] Castanheira L, Silva WO, Lima FHB, Crisci A, Dubau L, Maillard F. Carbon Corrosion in Proton-Exchange Membrane Fuel Cells: Effect of the Carbon Structure, the Degradation Protocol, and the Gas Atmosphere. ACS Catalysis. 2015;5:2184-94.
[30] Yu PT, Gu W, Makharia R, Wagner FT, Gasteiger HA. The Impact of Carbon Stability on PEM Fuel Cell Startup and Shutdown Voltage Degradation. ECS Transactions. 2006;3:797-809.
[31] Wang J, Yin G, Shao Y, Wang Z, Gao Y. Investigation of Further Improvement of Platinum Catalyst Durability with Highly Graphitized Carbon Nanotubes Support. J Phys Chem C. 2008;112:5784-9.
[32] Zhao X, Hayashi A, Noda Z, Kimijima Ki, Yagi I, Sasaki K. Evaluation of change in nanostructure through the heat treatment of carbon materials and their durability for the start/stop operation of polymer electrolyte fuel cells. Electrochim Acta. 2013;97:33-41.
[33] Ryoo R, Joo SH, Kruk M, Jaroniec M. Ordered Mesoporous Carbons. Adv Mater. 2001;13:677-81.
[34] Zeng J, Francia C, Dumitrescu MA, Monteverde Videla AHA, Ijeri VS, Specchia S, et al. Electrochemical Performance of Pt-Based Catalysts Supported on Different Ordered Mesoporous Carbons (Pt/OMCs) for Oxygen Reduction Reaction. Ind Eng Chem Res. 2012;51:7500-9.
[35] Zeng J, Francia C, Gerbaldi C, Baglio V, Specchia S, Aricò AS, et al. Hybrid ordered mesoporous carbons doped with tungsten trioxide as supports for Pt electrocatalysts for methanol oxidation reaction. Electrochim Acta. 2013;94:80-91.
[36] Calvillo L, Celorrio V, Moliner R, Cabot PL, Esparbé I, Lázaro MJ. Control of textural properties of ordered mesoporous materials. Microporous Mesoporous Mater. 2008;116:292-8.
[37] Calvillo L, Celorrio V, Moliner R, Lázaro MJ. Influence of the support on the physicochemical properties of Pt electrocatalysts: Comparison of catalysts supported on different carbon materials. Mater Chem Phys. 2011;127:335-41.
[38] Lázaro MJ, Calvillo L, Bordejé EG, Moliner R, Juan R, Ruiz CR. Functionalization of ordered mesoporous carbons synthesized with SBA-15 silica as template. Microporous Mesoporous Mater. 2007;103:158-65.

[39] Baglio V, Di Blasi A, Aricò AS, Antonucci V, Antonucci PL, Nannetti F, et al. Investigation of the electrochemical behaviour in DMFCs of chabazite and clinoptilolite-based composite membranes. Electrochim Acta. 2005;50:5181-8.
[40] Antonucci PL, Romeo F, Minutoli M, Alderucci E, Giordano N. Electrochemical corrosion behavior of carbon black in phosphoric acid. Carbon. 1988;26:197-203.
[41] Maass S, Finsterwalder F, Frank G, Hartmann R, Merten C. Carbon support oxidation in PEM fuel cell cathodes. J Power Sources. 2008;176:444-51.
[42] Lázaro MJ, Celorrio V, Calvillo L, Pastor E, Moliner R. Influence of the synthesis method on the properties of Pt catalysts supported on carbon nanocoils for ethanol oxidation. J Power Sources. 2011;196:4236-41.
[43] Calvillo L, Celorrio V, Moliner R, Garcia AB, Caméan I, Lazaro MJ. Comparative study of Pt catalysts supported on different high conductive carbon materials for methanol and ethanol oxidation. Electrochim Acta. 2013;102:19-27.
[44] Long NV, Duy Hien T, Asaka T, Ohtaki M, Nogami M. Synthesis and characterization of Pt–Pd alloy and core-shell bimetallic nanoparticles for direct methanol fuel cells (DMFCs): Enhanced electrocatalytic properties of well-shaped core-shell morphologies and nanostructures. Int J Hydrogen Energy. 2011;36:8478-91.
[45] Kinoshita K, Bett J. Electrochemical oxidation of carbon black in concentrated phosphoric acid at 135°C. Carbon. 1973;11:237-47.
[46] Miyake H, Okada T, Samjeske G, Osawa M. Formic acid electrooxidation on Pd in acidic solutions studied by surface-enhanced infrared absorption spectroscopy. Phys Chem Chem Phys. 2008;10:3662-9.